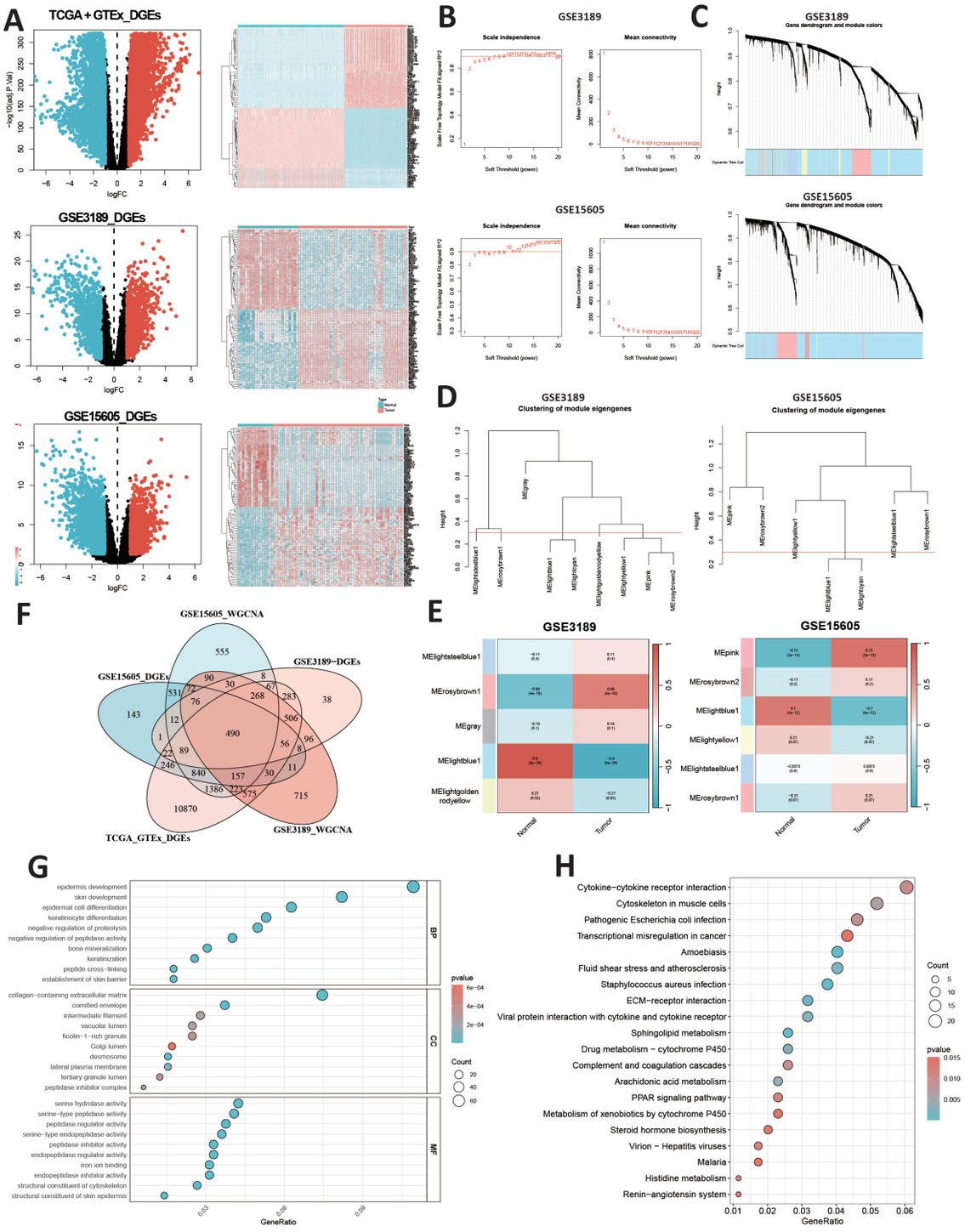

Figure S1 Identification of DEGs in tumor versus normal tissues. (A) Volcano plots displaying DEGs in TCGA and GTEx datasets, GSE3189, and GSE15605. The x-axis represents log2 fold change (log2FC), and the y-axis shows the negative log10-adjusted P value [−log10(adj. P)]. Red and blue dots denote significantly upregulated and downregulated genes, respectively (adjusted P<0.05, |log2FC| >1). Heatmaps below illustrate expression patterns of DEGs in normal (N) and tumor (T) tissues. (B) Analysis of scale-free gene network topology and mean connectivity across soft-threshold powers in the GSE3189, and GSE15605 datasets cohort. (C) Dendrogram showing the differential gene clustering based on topological overlap in the GSE3189, and GSE15605 datasets. (D) Clustering of consensus module eigengenes for the GSE3189, and GSE15605 datasets, where genes with correlations between modules > 0.9 below the red line were merged. (E) Weighted gene co-expression network analysis (WGCNA) of GSE3189 and GSE15605. Heatmaps depict module-trait associations between module eigengenes (MEs) and tissue type (normal vs. tumor). Color intensity indicates correlation strength (P<0.05). (F) Venn diagram showing overlapping DEGs among TCGA_GTEx_DEGs, GSE15605_DEGs, GSE3189_DEGs, GSE3189_WGCNA, and GSE15605_WGCNA. (G-H) Functional enrichment analysis of consensus DEGs: (G) GO terms and (H) KEGG pathways. Dot size reflects the number of enriched genes, and color indicates significance. DEG differentially expressed genes; GO, Gene Ontology; KEGG, Kyoto Encyclopedia of Genes and Genomes.

© AME Publishing Company.
https://dx.doi.org/10.21037/tcr-2025-aw-2548

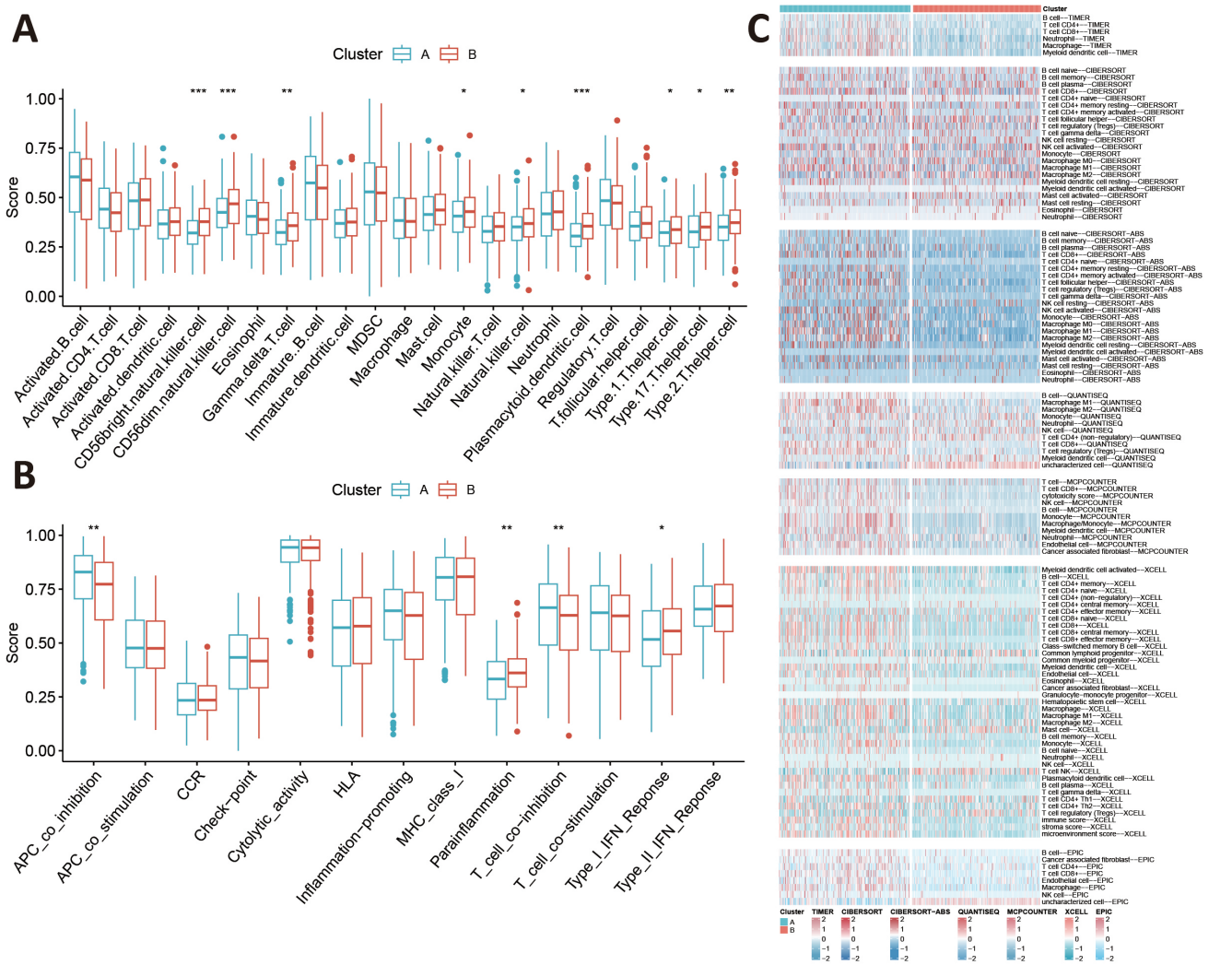

Figure S2 Immune cell infiltration analysis. (A,B) Box plots illustrating the differences in immune cell infiltration (A) and immune-related functions (B) in Cluster A and B subgroups, displaying the distribution of different immune cell scores and immune function scores. (C) Expression heatmaps of Cluster A and Cluster B subgroups generated via immune cell infiltration analysis using 7 tools, where color gradients represent differences in gene expression levels, with molecule names annotated on the right and the legend below clarifying the corresponding relationship between color and expression level. *, P<0.05; **, P<0.01; ***, P<0.001; ****, P<0.0001; ns, not significant.

© AME Publishing Company.
https://dx.doi.org/10.21037/tcr-2025-aw-2548

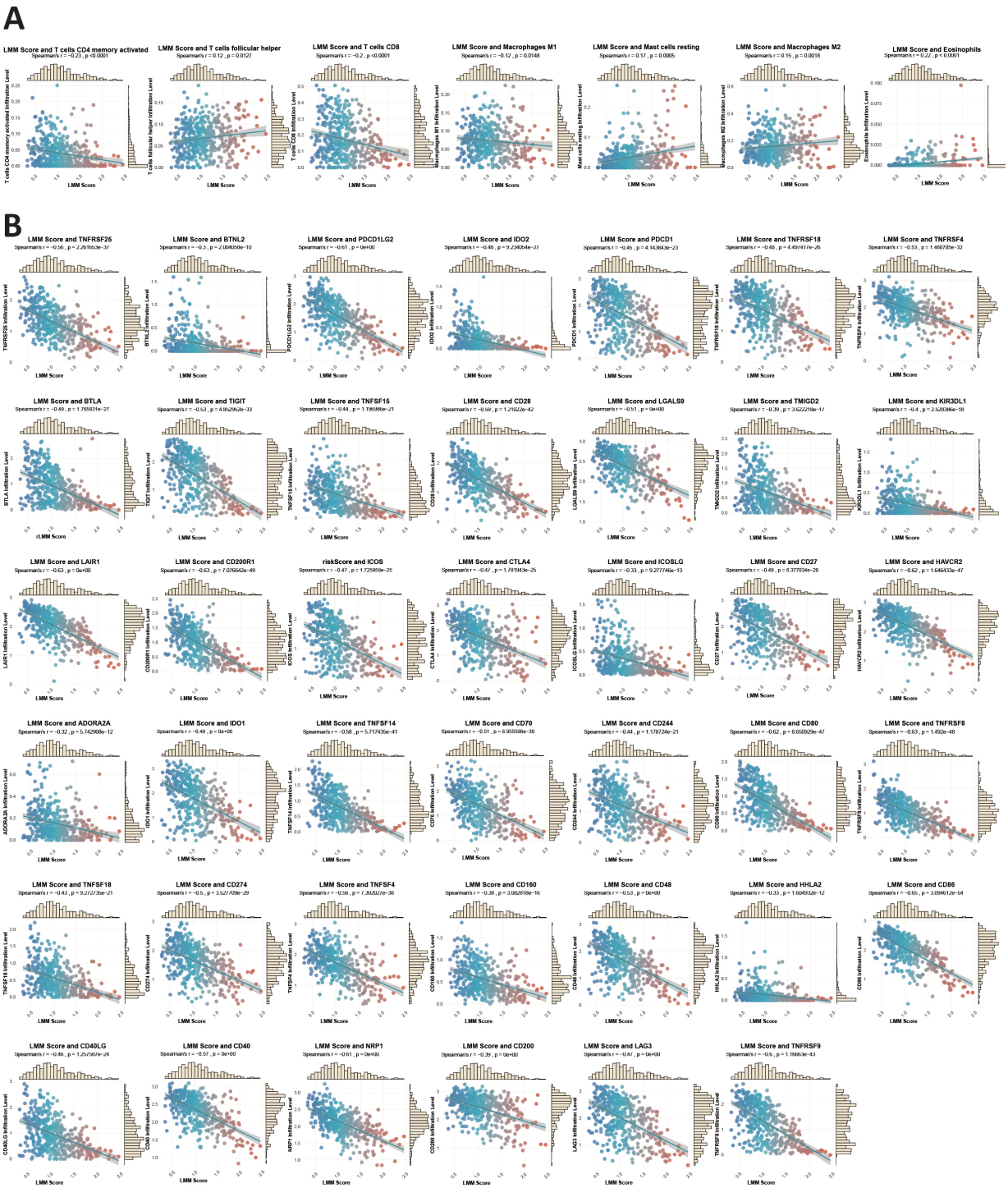

Figure S3 Correlation analysis of LMM score with immune infiltration and immune checkpoints. (A) Correlations between the LMM score and the abundances of immune cells. (B) Correlations between the LMM score and the immune checkpoint genes. *, P<0.05; **, P<0.01; ***, P<0.001; ****, P<0.0001; ns, not significant. LMM, Lipid metabolism molecular.

© AME Publishing Company.
https://dx.doi.org/10.21037/tcr-2025-aw-2548

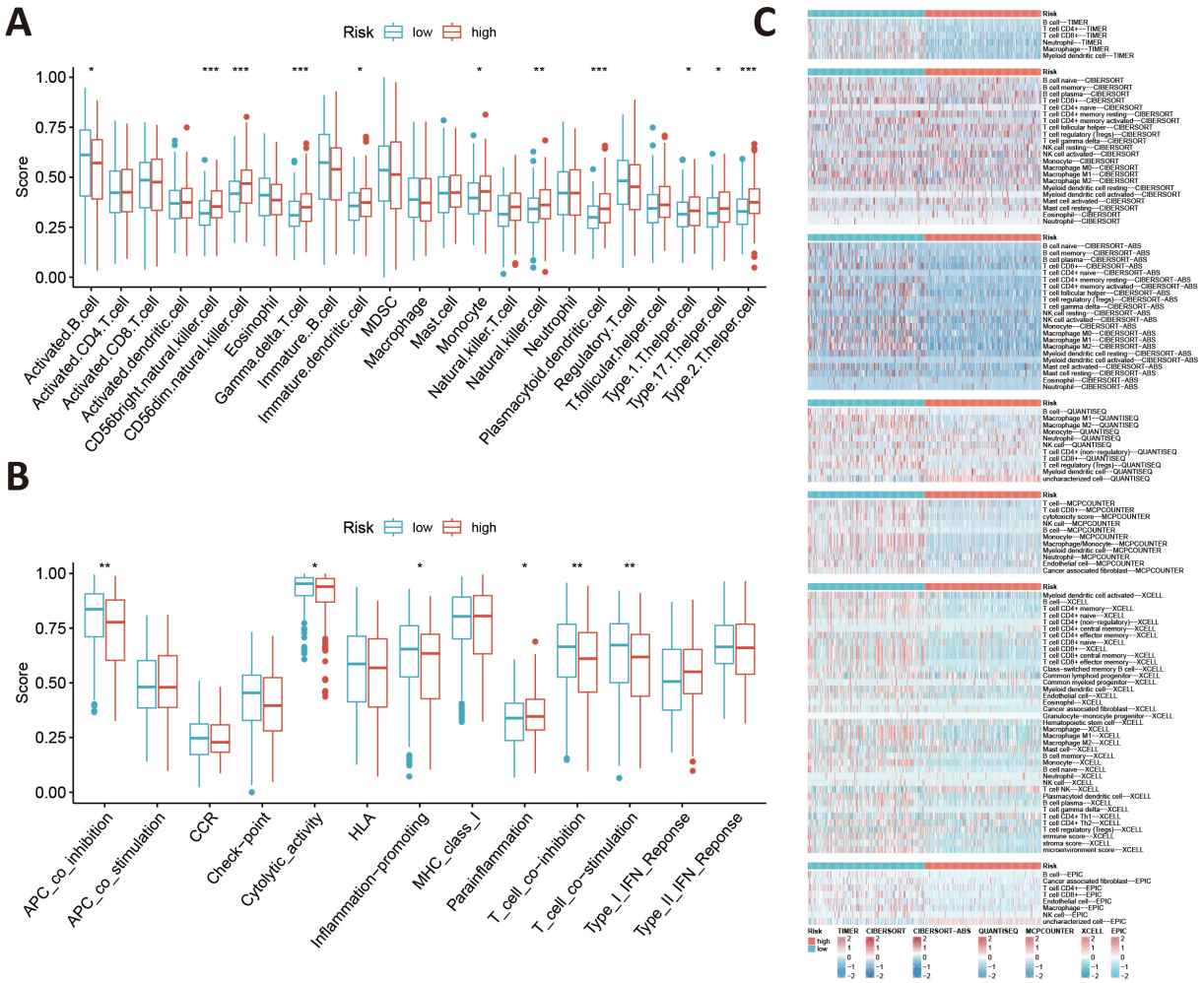

Figure S4 Immune cell infiltration analysis. (A,B) Box plots illustrating the differences in immune cell infiltration (A) and immune-related functions (B) in low-risk and high-risk subgroups, displaying the distribution of different immune cell scores and immune function scores. (C) Expression heatmaps of low-risk and high-risk subgroups generated via immune cell infiltration analysis using 7 tools, where color gradients represent differences in gene expression levels, with molecule names annotated on the right and the legend below clarifying the corresponding relationship between color and expression level. *, P<0.05; **, P<0.01; ***, P<0.001; ****, P<0.0001; ns, not significant.

© AME Publishing Company.
https://dx.doi.org/10.21037/tcr-2025-aw-2548

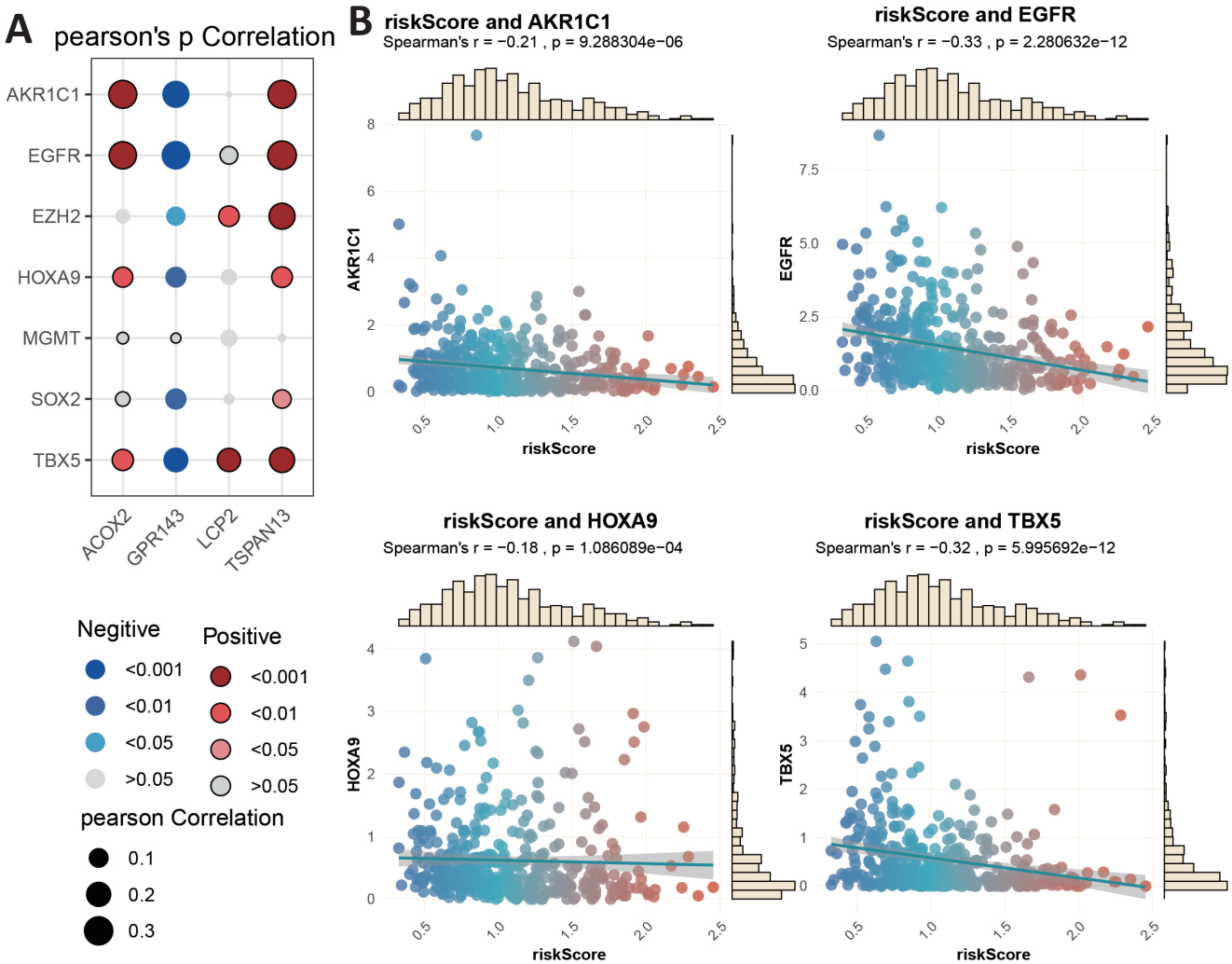

Figure S5 The correlation between the Risk score and chemotherapy sensitivity-related genes. (A) Correlations between the prognostic model genes and the chemotherapy sensitivity-related genes. (B) The scatter plots displaying the correlative relationship between the chemotherapy sensitivity-related genes and risk score value.

© AME Publishing Company.
https://dx.doi.org/10.21037/tcr-2025-aw-2548

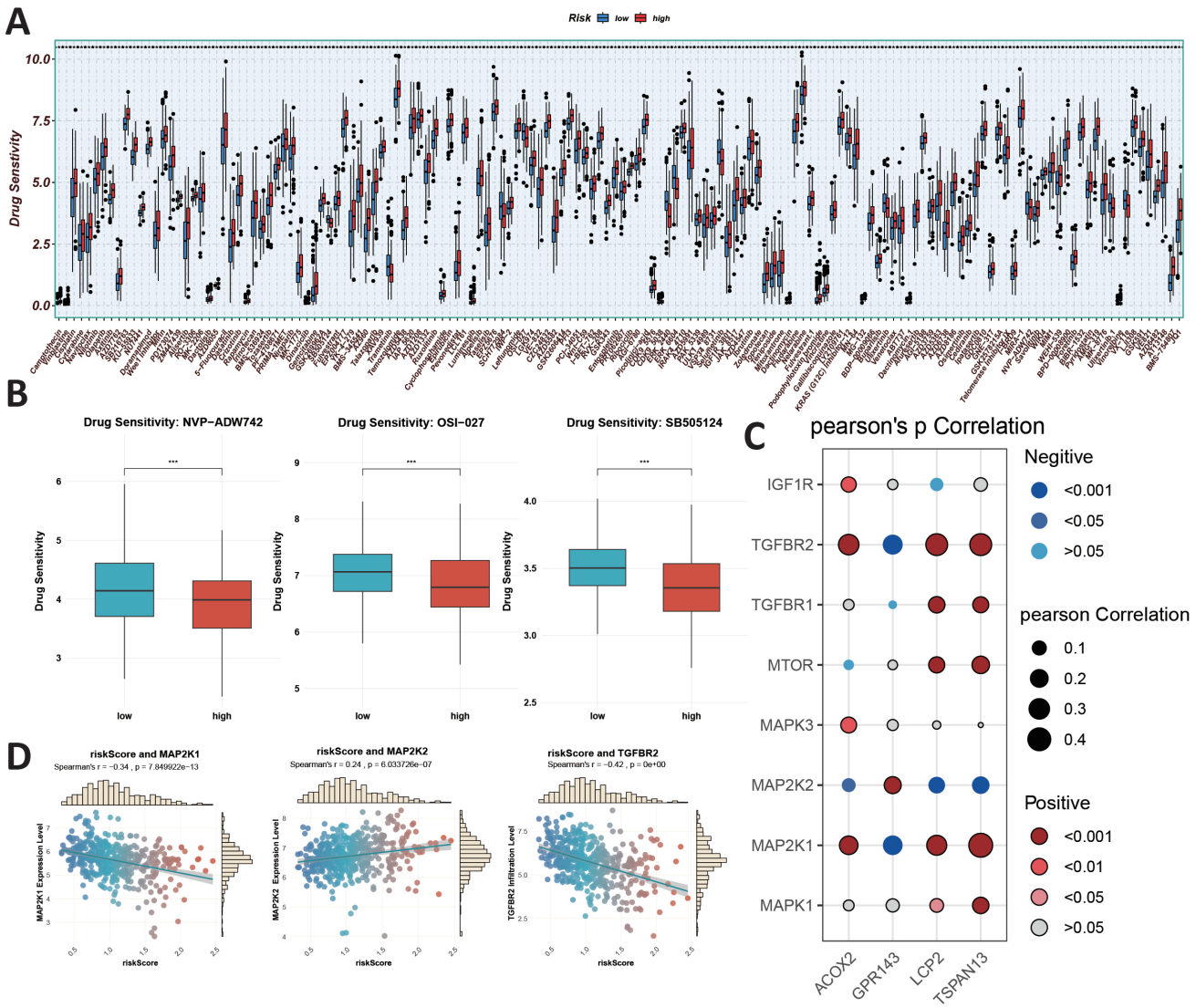

Figure S6 The correlation between the Risk score and drug targets. (A) Comparison of the drug sensitivity differences between two subgroups. (B) Box plots showing drug sensitivity differences of TGF targeted drugs, IGF1R targeted drugs and mTOR targeted drugs. (C) Correlations between the prognostic model genes and the drug targets. (D) The scatter plots displaying the correlative relationship between the drug targets and risk score value. *, P<0.05; **, P<0.01; ***, P<0.001; ****, P<0.0001; ns, not significant.

© AME Publishing Company.
https://dx.doi.org/10.21037/tcr-2025-aw-2548

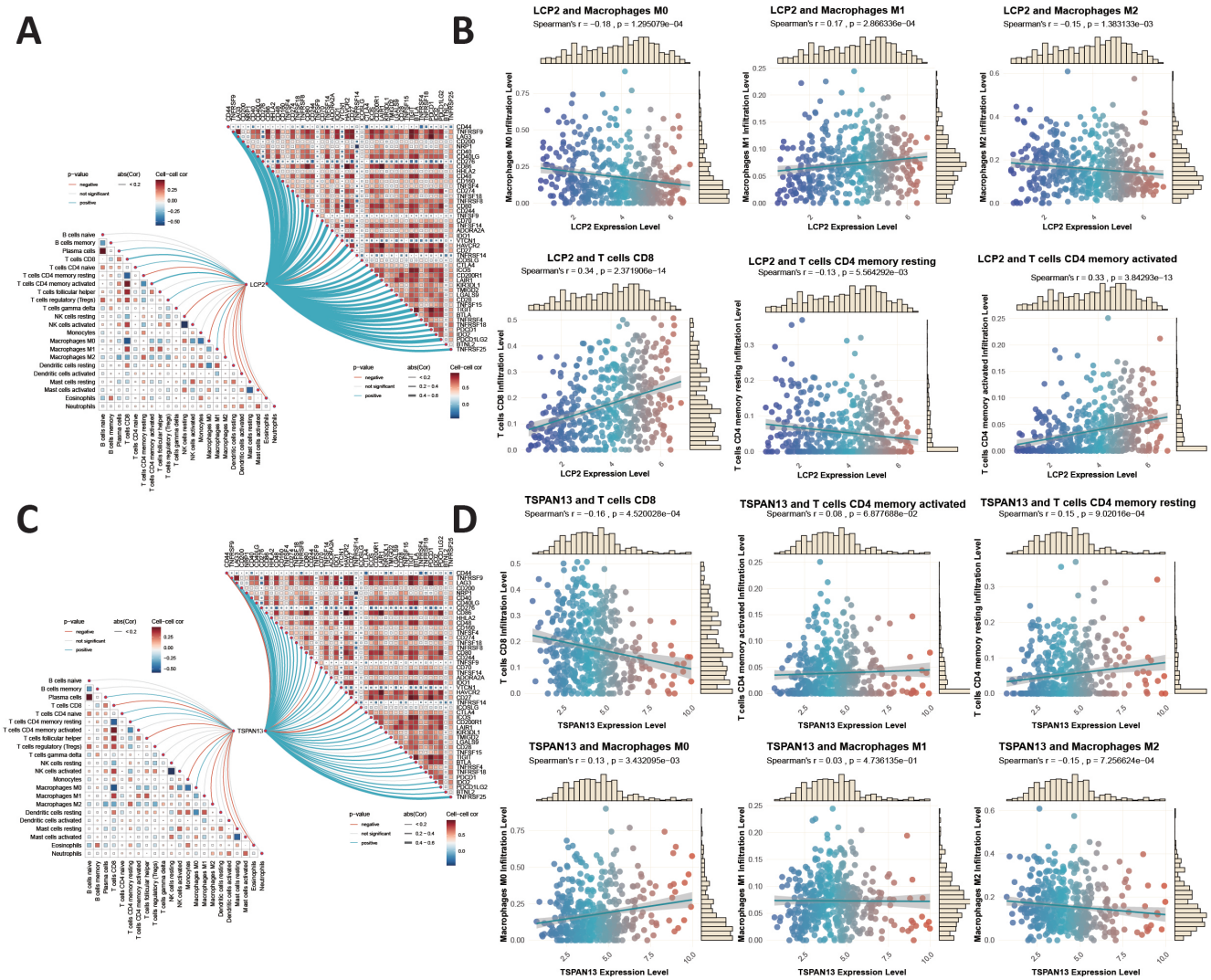

Figure S7 The correlation between the Risk score and drug targets. (A) Correlations between the prognostic model genes and the drug targets. (B) The scatter plots displaying the correlative relationship between the drug targets and risk score value.

© AME Publishing Company.
https://dx.doi.org/10.21037/tcr-2025-aw-2548

Figure S8 Expression locations of LCP2, TSPAN13, and ACOX2 in the immune landscape Visualization of single-cell analysis results based on different cutaneous melanoma (SKCM) datasets, including GSE14190 (A), GSE19249 (B), GSE123130 (C), GSE16979_aPD1 (D), and GSE72068 (E). The left column shows the cell type annotations of each dataset, and the middle and right columns present the expression distributions of LCP2, TSPAN13, and ACOX2 genes at the single-cell level, with the color gradient reflecting the differences in gene expression levels.

© AME Publishing Company.
https://dx.doi.org/10.21037/tcr-2025-aw-2548